Buenos Aires – 5 to 9 September, 2016
Acoustics for the 21st Century…

PROCEEDINGS of the 22nd International Congress on Acoustics

Biomedical Acoustics: Paper ICA2016-651

Detecting breast cancer with high-frequency (20-80 MHz) ultrasound: A histological perspective

Timothy Doyle[(a)]

[(a)] Utah Valley University, United States, timothy.doyle@uvu.edu

Abstract

The development of intraoperative methods to detect breast cancer in excised tissue specimens is a crucial priority in breast conservation surgery (BCS). A finding of cancer in tissue margins (the boundary between resected and unresected tissue) by pathology analysis after surgery indicates that some of the cancer was missed during BCS and the patient must return for additional surgery. Evaluating sentinel lymph node status during surgery is also critical since it determines the need for axillary lymph node dissection. High-frequency ultrasound has been found to display high sensitivity and specificity for malignant tissue in BCS margin specimens and lymph nodes. The method uses through transmission of narrow pulses centered at 50 MHz, yielding a broad spectral response of the tissue sample. The received pulses produce noise-free spectra that vary in shape with tissue pathology. BCS specimen data indicate that the peak density of the spectrum (the number of peaks and valleys in the 20-80 MHz band) correlates with breast tissue histology, but not with mammographic tissue density. Experiments with histology mimicking phantoms containing microspheres and fibers show that peak density is insensitive to fibrous microstructures but strongly correlates to microsphere size. Computer simulations of forward scattering from lobular carcinoma *in situ* models show that peak density increases with tumor progression, but also suggest that peak density arises from scattering resonances with cells. Thus, the sensitivity of peak density to cancerous tissue may be due to structural differences between malignant and normal cells. Whether it characterizes small-scale tissue structure or cell properties, peak density offers a promising window into the histology and detection of breast cancer.

Keywords: High-frequency ultrasound, breast cancer

Detecting breast cancer with high-frequency (20-80 MHz) ultrasound: A histological perspective

1 Introduction

A majority of breast cancer patients (60-75%) choose breast conservation surgery (BCS) for their surgical treatment because it preserves unaffected breast tissue, is less invasive than mastectomy, and is considered an equally effective treatment option when accompanied with radiation therapy [1]. However, 20-60% of these women will require a second or third surgery in order to excise residual cancer left behind in the breast after the initial surgery [1,2]. Currently, surgeons send removed tissue from BCS to a pathology lab for analysis where microscopically thin slices (sections) are inspected to confirm that the surgeon obtained a negative (cancer-free) edge or margin around the removed tumor. This process takes several days. If cancer is found in the margin, it is likely that some of the cancer was missed and the patient must return for additional surgery. Not only is a repeat surgery expensive, it inflicts pain, discomfort, and emotional hardship on the patient. It also requires extra time to heal from an additional surgery.

Similarly, evaluating the status of the sentinel lymph nodes (SLNs) is critical to determining whether the cancer has metastasized and if further surgery is required. If malignant tissue is discovered in one or more SLNs beyond a few isolated tumor cells, then axillary lymph node dissection (ALND) is required [3]. ALND is the removal of all or most of the lymph nodes from under the patient's arm. Since SLNs are typically evaluated under the microscope in the pathology lab, much like surgical margins, ALND often occurs as a second surgery. As with the problem with surgical margins, an intraoperative technique for assessing SLN status would, therefore, substantially relieve patient hardship as well as reduce medical costs. It should be noted that ALND is becoming more regarded as an aggressive procedure, and has a high rate of serious complications such as lymphedema (~25%), shoulder dysfunction, wound infection, nerve damage, numbness, and chronic pain [4].

The problem of high BCS re-excision rates, combined with the need to rapidly determine SLN status during surgery, is consequently driving a significant effort into the development of real-time, noninvasive methods to evaluate surgical specimens directly in the operating room. A number of methods are, therefore, being investigated for the intraoperative evaluation of margin status, including specimen radiography [5], magnetic resonance imaging [6], nuclear imaging [7], electromagnetic sensing [8], optical spectroscopy [9-11], optical coherence tomography (OCT) [12-14], and ultrasonic methods [15]. Many of these methods have limitations, such as the shallow penetration depth of optical methods into tissue (2-4 mm), or the challenges of using radioactive tracers in nuclear imaging. Methods are also being developed for the intraoperative assessment of SLNs, including frozen section analysis, imprint cytology, qRT-PCR, and one-step nucleic acid amplification (OSNA) [3,16]. Frozen section analysis and imprint cytology are also applied to margin assessments.

Research has shown that high-frequency (HF) ultrasound in the 20-80 MHz range offers a viable approach for intraoperative specimen assessment. In contrast to conventional medical

ultrasound, the frequency range of HF ultrasound produces sound waves with wavelengths that span sizes from those of cells (19 μm for 80 MHz) to those of small tissue structures in the breast (75 μm for 20 MHz), such as ductules and lobules. Since acoustic scattering is most efficient when the wavelength is close in size to the scattering structure, HF ultrasound is highly sensitive to differences in cell and tissue microstructures. Additionally, the use of spectral analysis with HF ultrasound permits the differentiation of tissue pathology. This is in contrast to conventional ultrasound, radiology, or nuclear imaging, where image interpretation, contrast agents, and targeted biomarkers are predominantly used.

Traditionally, HF ultrasound has been associated with scanning acoustic microscopy (SAM). While SAM has shown promise for differentiating malignant from non-malignant breast cancer in frozen sections (80-200 MHz) and cells suspended in fluids (400 MHz) [17,18], it is not suited for the rapid evaluation of fresh tissue specimens.

Quantitative ultrasound (QUS) analyzes the spectra from backscatter (echo) signals from ultrasound images to derive parameters that can differentiate tissue pathology. The analyses may be either empirical or use scattering models to estimate parameters such as the effective scatter diameter (ESD), effective acoustic concentration (EAC), and spacing among scatterers (SAS) [19,20]. A study of 42 patients with locally advanced breast cancer yielded an accuracy of 83% for differentiating malignant from non-malignant tissue using ultrasound images acquired at a 6-MHz center frequency and a combination of ESD, EAC, and SAS [20]. QUS can also be applied to the evaluation of surgical specimens using HF ultrasound. In a study of 112 SLNs from 77 patients with colorectal cancer, SLNs were scanned in three dimensions using a 25.6-MHz center frequency [21]. Analysis of the data using a combination of ESD and *k*, the ratio of the coherent to incoherent content of the signal, provided a sensitivity of 95.0% and a specificity of 95.7% for detecting malignant SLNs.

This paper reviews the utility and histological significance of a HF ultrasound parameter specific to surgical specimens: Peak density. Peak density is the number of peaks (maxima) and valleys (minima) in a specified frequency band of the power spectrum of a HF ultrasound signal. Peak density is a relatively new and unknown spectral parameter that is obtained from coherent, broadband ultrasonic signals and has been found to correlate with breast tissue pathology [15]. This paper describes the ultrasonic measurements and data analysis method required for finding peak density. Peak density results from breast cancer specimen studies, phantom experiments, and computational models will also be presented. Finally, the effects of breast tissue histology and cell structure on peak density will be summarized.

2 Methods

Peak density is obtained from coherent ultrasound signals that have propagated through a tissue specimen. Figure 1 displays the through-transmission measurement configuration required for acquiring the coherent signals. Narrow HF pulses (broadband in the frequency domain) are generated by the transmit transducer, propagated through the tissue, and captured by the receive transducer. Acoustic scattering within the tissue modifies the frequency components of the pulses by preferentially scattering specific frequencies. This preferential

scattering produces structure in the ultrasonic spectrum. This structure is directly analogous to extinction in optical scattering, and is dependent on the size, shape, and spatial distribution of the scatterers.

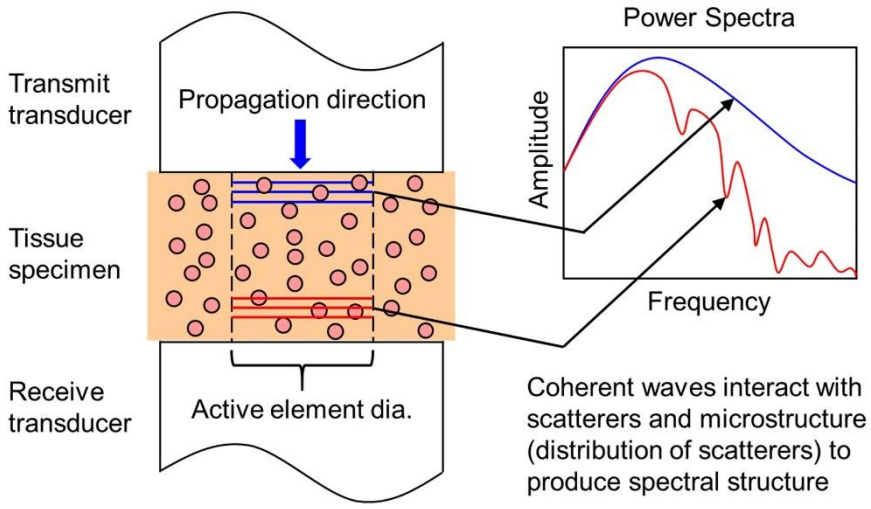

Figure 1: Configuration for measuring peak density

In studies performed on BCS surgical specimens, the measurements were acquired with the use of two 50-MHz immersion transducers (Olympus NDT, V358-SU, 12.7-mm OD, 6.35-mm active element diameter), a HF square-wave pulser/receiver (UTEX, UT340), and either a 500-MHz (Hewlett-Packard, HP-54522A) or 1-GHz (Agilent, DSOX3104A) digital oscilloscope. An aluminum test fixture supported the tissue specimen and held the transducers in contact with the sample. Ultrasonic waveforms were averaged in the signal acquisition and specimen thickness was recorded for each measurement. During ultrasonic testing, each specimen was placed inside a resealable plastic storage bag to protect the specimen from contamination, and the outside of the bag was coupled to the transducers with either ultrasound scanning gel or glycerol. One to five positions were tested on each specimen based on specimen size.

BCS surgical specimens were tested in a 2010 pilot study with 34 margin specimens from 17 patients, and in a 2013-2014 validation study with 349 margin specimens from 73 patients. The validation study also included a sub-study comprising 78 lymph nodes from 39 patients. Ultrasonic testing of tissue specimens was performed during the course of routine BCS at the Huntsman Cancer Institute (HCI) in accordance with the ethical principles and guidelines for human subjects research. These included approval by the University of Utah Institutional Review Board (IRB 00037350 and 00062775) and informed consent from patients. Specimens ranged from 1-5 cm in length and width, 0.2-1.5 cm in thickness, and did not require any additional procedures or resection that affected the patient or surgical outcome. Specimens were tested immediately following resection. Routine pathology was performed on the specimens after ultrasonic testing and the findings were correlated to the ultrasonic results.

Because of the small wavelength of the transmitted ultrasound (30 μm for 50 MHz) in comparison to the size of the active element (6.35 mm), the transmit transducer produced coherent plane-wave pulses which propagated through the tissue to the receive transducer.

Figure 2(a) is an example of a coherent ultrasonic waveform after propagating though a BCS margin specimen with normal pathology. Peak densities were derived from the time-domain waveforms by performing a Fourier transform and counting the number of peaks and valleys in the 20-80 MHz region of the resulting power spectra [Figure 2(b)]. Attenuations were calculated by scaling the waveforms to account for receiver gain and tissue thickness, and using a Hilbert transform to obtain the waveform envelopes and their corresponding amplitudes.

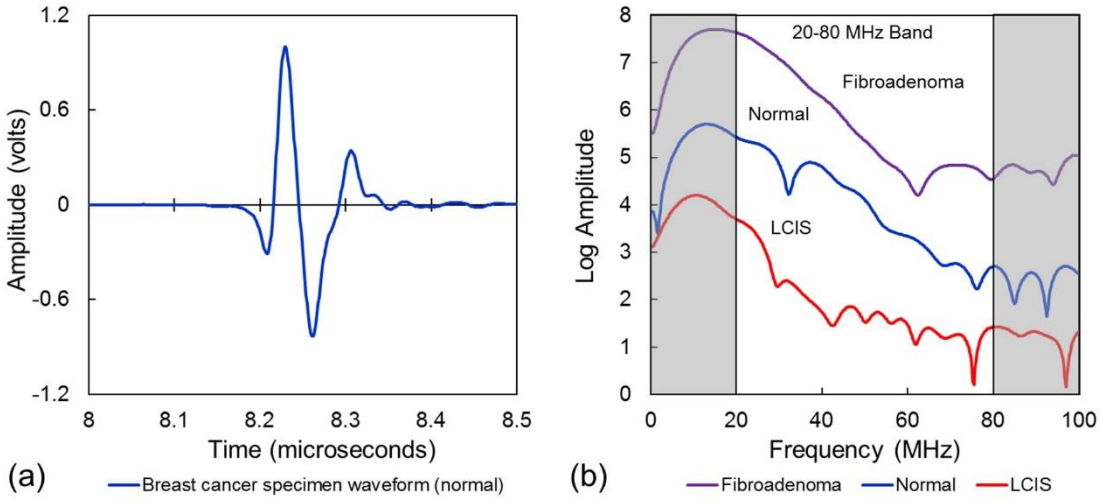

Figure 2: HF through-transmission waveform of BCS margin specimen (a) and ultrasonic spectra showing variations in peak density with pathology (b).

The ultrasonic spectra in Figure 2(b) reveal different levels of structure, and therefore peak density, between the fibroadenoma, normal, and lobular carcinoma *in situ* (LCIS) specimens. Analysis of the pilot study data, Figure 3(a), revealed that peak density correlated with breast tissue pathology [15]. The analysis showed that peak density most closely matched five broad tissue categories corresponding to (1) fat necrosis, fibroadenomas, and tubular adenomas (FA-FN); (2) normal tissue (Normal); (3) atypical pathologies including benign calcifications, atypical ductal hyperplasia, fibrocystic changes, and benign papilloma (Benign); (4) ductal carcinomas, *in situ* and invasive (DC); and (5) lobular carcinomas, *in situ* and invasive (LC). Attenuation, Figure 3(b), showed less of a correlation to these five pathology categories.

In addition to surgical specimen studies, peak density studies were also performed with histology mimicking phantoms and computational models. The phantoms were created from a matrix of distilled water, agarose powder, and 10X TBE stock solution. Polyethylene microspheres and fibers were embedded into the agarose matrix to simulate breast tissue microstructures such as lobules and ductules. HF ultrasonic measurements were acquired from the phantoms using the same method as for surgical specimens. The computational models used a multipole expansion approach, which simulated HF elastic wave scattering at the cellular level [22]. Cells and nuclei were modeled as spheres arranged into lobules and other micro-structures. Spherical wave functions, boundary conditions, and addition theorems were used to fully simulate multiple scattering within micro-regions of tissue containing up to 2075 cells.

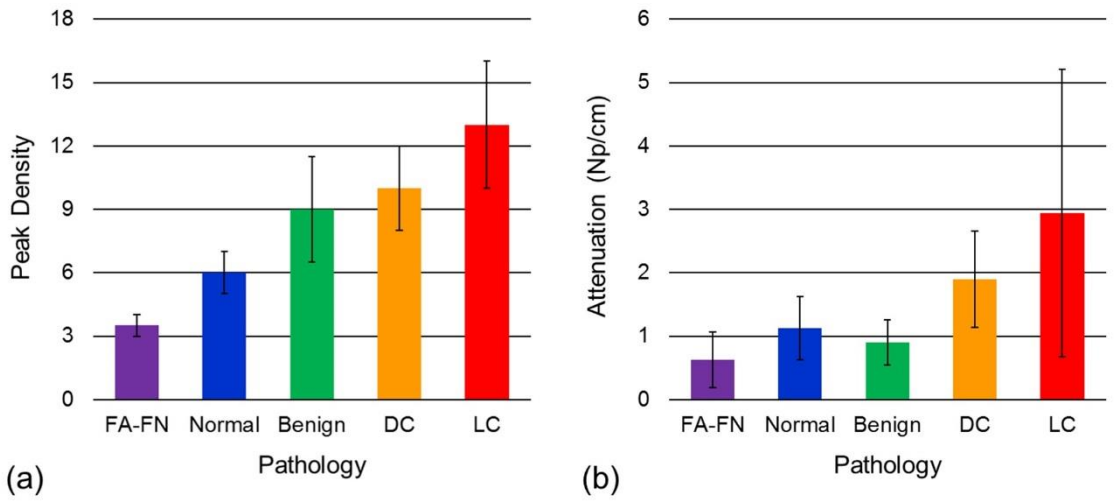

Figure 3: Correlation of breast tissue pathology with peak density (a) and attenuation (b).

3 Results

3.1 Binary Classification Results from Surgical Studies

Table 1 lists the statistical measures for the 2010 study with margins, the 2014 study with margins, and the 2014 study with lymph nodes. Statistical measures were calculated with respect to malignant versus non-malignant findings. Parameters compared are peak density, attenuation, and a combination of the two using a multivariate analysis. The results show that peak density and the multivariate analysis have a consistent range of accuracy values (71.1-79.5% and 72.7-83.3%, respectively). In contrast, the accuracy values for attenuation vary to a much greater degree, with a range of 43.6-77.4%. Sensitivity and specificity show similar trends, with greater consistency and robustness for peak density and the multivariate analysis.

Table 1: Comparison of statistical measures for peak density, attenuation, and multivariate analysis for three breast cancer studies.

Study	Parameter	Accuracy	Sensitivity	Specificity
2010-Margins	Peak Density	71.7	69.2	74.1
	Attenuation	77.4	57.7	96.3
	Multivariate	81.1	76.9	85.2
2014-Margins	Peak Density	71.1	73.9	71.0
	Attenuation	60.0	73.9	59.5
	Multivariate	72.7	82.6	72.3
2014-Lymph Nodes	Peak Density	79.5	62.5	81.4
	Attenuation	43.6	50.0	42.9
	Multivariate	83.3	87.5	82.9

3.2 Effect of Mammographic Breast Density on Peak Density

Figure 4 shows the correlation between mammographic breast density, obtained from patient mammograms in the 2014 margin study, with peak density and attenuation measurements from surgical specimens. Unsurprisingly, attenuation exhibits a linear trend with breast density. In contrast, peak density shows no trend with breast density. These results demonstrate that peak density and attenuation are independent parameters, arising from different mechanisms within the tissue. Studies with histology mimicking phantoms containing polyethylene fibers confirmed these results, with peak density insensitive to the density of fibers in the phantom, but with attenuation displaying a linear trend with fiber density. The results also further support the use peak density as a principal parameter for detecting malignant breast pathology, due to its insensitivity to breast density, a patient-specific factor that often hinders breast cancer detection.

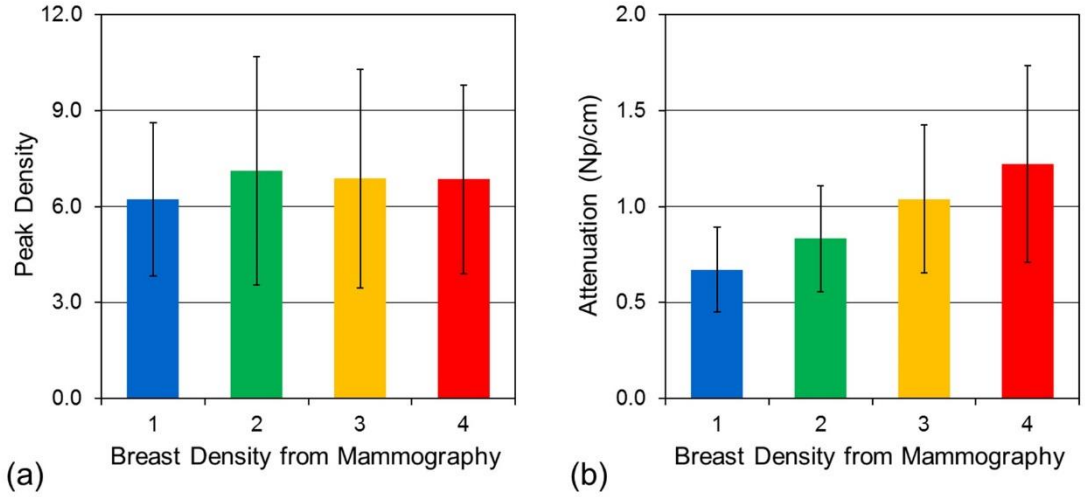

Figure 4: Correlation of mammographic breast density with peak density (a) and attenuation (b). (1 = almost entirely fat; 2 = scattered areas of fibroglandular density; 3 = heterogeneously dense; 4 = extremely dense).

3.3 Effect of Scatterer Size on Peak Density

In addition to fibers, phantoms were also prepared containing polyethylene microspheres with constant weight percent (0.8%) and with diameters varying by sample. Figure 5 shows that both peak density and attenuation varied with microsphere diameter. However, peak density followed an inverse particle size relationship, whereas attenuation increased linearly as microsphere diameter decreased. A second experiment with constant microsphere diameter (98 μm), but varying concentration, showed no significant trend for peak density, but a linear trend for attenuation with inclusion weight percent. The experiments indicate that peak density arises principally from scattering at the microscopic level, whereas attenuation is sensitive to concentration. Figure 5(a) demonstrates that peak density does not begin to show a response until the microsphere size decreases to the same scale as the ultrasound wavelength in the material (60-100 μm for 15-25 MHz). Peak density is also independent of specimen thickness, further demonstrating that it is sensitive mainly to scatterer size. The attenuation results are most likely due to an increase in inclusion concentration (as inclusion size decreases, inclusion number increases for a fixed volume of inclusions).

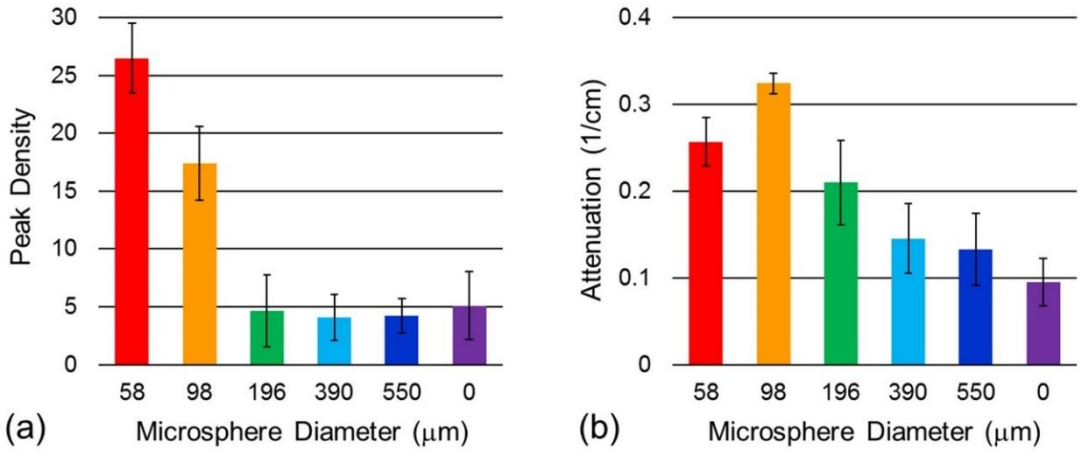

Figure 5: Peak density (a) and attenuation (b) of phantom specimens containing microspheres.

3.4 Cell-Level Computer Modeling of Peak Density and LCIS

Figure 6 shows results from a computer model of ultrasonic wave propagation through breast tissue at various stages of LCIS. Figure 6(a) displays the growth of peaks between 50-70 MHz (particularly the large peak at 65 MHz) as lobules are infiltrated with malignant cells (modeled with larger nuclear and cell radii than normal cells). Figure 6(b) displays the corresponding peak densities from the spectra, exhibiting values consistent with those from surgical specimens [Figure 3(a)]. Comparison of the simulated spectra with those from previous models indicate that the changes arise primarily from alteration of the microstructure of the simulated tissue, and not from changes in cell structure [22]. Previous simulations that only altered the microstructure of normal cell ensembles, such as by aggregation into foam-like microstructures with lobule-like cavities, produced very similar spectral results, but in reverse. As cavities formed in initially uniform tissue, a large peak at 67 MHz was quenched [22]. The spectral changes in Figure 6(a), therefore, can be ascribed solely to the vanishing of the lobular cavities due to infiltration.

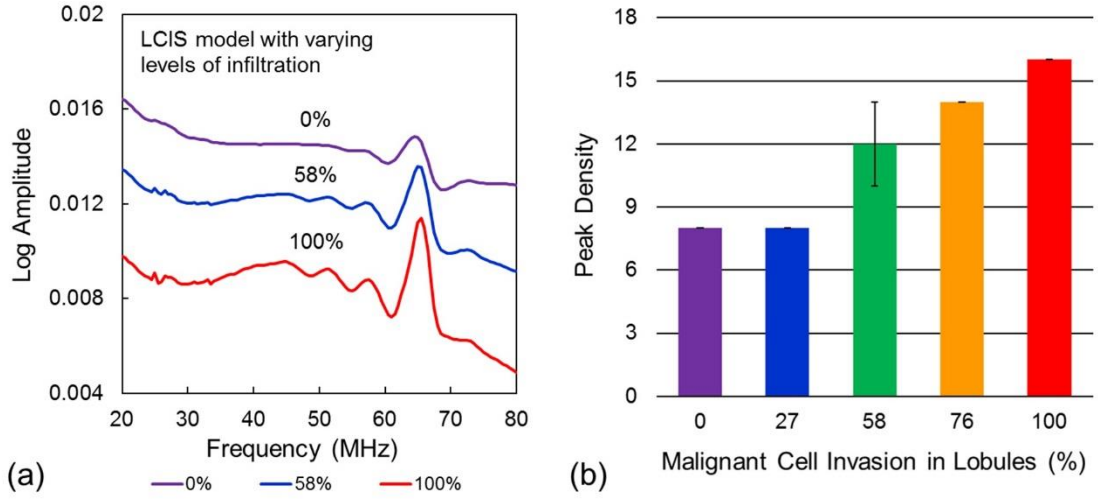

Figure 6: Spectra (a) and peak density results (b) from a computer model of LCIS.

4 Conclusions

Peak density is an ultrasonic spectral parameter developed for use with coherent ultrasonic signals. Results from three surgical studies consisting of 456 specimens from 90 patients demonstrate that peak density is sensitive to glandular and lymph node tissue pathology in the breast, but is insensitive to fibroglandular breast density. Supplementary experiments with histology mimicking phantoms provide evidence that peak density arises primarily from scattering at the microscopic level. Computational models indicate that modifications to tissue microstructures such as lobules are mainly responsible for changes in peak density. The results to date reveal that peak density offers a histology-based approach into the ultrasonic detection of breast cancer.

Acknowledgments

This research was funded by grants from the National Cancer Institute (NIH Award Number R21CA131798), the Elsa U. Pardee Foundation, the Eppley Foundation for Research, the State of Utah (Technology Commercialization and Innovation Program), and Utah Valley University.

References

[1] McCahill, L.; Single, R.; Aiello Bowles, E.; Feigelson, H.; James, T.; Barney, T.; Engel, J.; Onitilo, A. Variability in reexcision following breast conservation surgery. *Journal of the American Medical Association*, Vol 307 (5), 2012, pp 467-475.

[2] Waljee, J.; Hu, E.; Newman, L.; Alderman, A. Predictors of re-excision among women undergoing breast-conserving surgery for cancer. *Annals of Surgical Oncology*, Vol 15 (5), 2008, pp 1297-1303.

[3] Huxley, N.; Jones-Hughes, T.; Coelho, H.; Snowsill, T.; Cooper, C.; Meng, Y.; Hyde, C; Mújica-Mota, R. A systematic review and economic evaluation of intraoperative tests [RD-100i one-step nucleic acid amplification (OSNA) system and Metasin test] for detecting sentinel lymph node metastases in breast cancer. *Health Technology Assessment*, Vol 19 (2), 2015, pp 1-215.

[4] Lyman, G.; Temin, S.; Edge, S.; Newman, L.; Turner, R.; Weaver, D.; Benson, A.; Bosserman, L.; Burstein, H.; Cody, H.; Hayman, J.; Perkins, C.; Podoloff, D.; Giuliano, A. Sentinel lymph node biopsy for patients with early-stage breast cancer: American Society of Clinical Oncology clinical practice guideline update. *Journal of Clinical Oncology*, Vol 32 (13), 2014, pp 1365-1386.

[5] Bathla, L.; Harris, A.; Davey, M.; Sharma, P.; Silva, E. High resolution intra-operative two-dimensional specimen mammography and its impact on second operation for re-excision of positive margins at final pathology after breast conservation surgery. *American Journal of Surgery*, Vol 202 (4), 2011, pp 387-394.

[6] Abe, H.; Shimauchi, A.; Fan, X.; River, J.; Sattar, H.; Mueller, J.; Karczmar, G.; Newstead, G. Comparing post-operative human breast specimen radiograph and MRI in lesion margin and volume assessment. *Journal of Applied Clinical Medical Physics*, Vol 13 (6), 2012, pp 267-276.

[7] Das, S.; Thorek, D.; Grimm, J. Cerenkov imaging. *Advances in Cancer Research*, Vol 124, 2014, pp 213-234.

[8] Schnabel, F.; Boolbol, S.; Gittleman, M.; Karni, T.; Tafra, L.; Feldman, S.; Police, A.; Friedman, N.; Karlan, S.; Holmes, D.; Willey, S.; Carmon, M.; Fernandez, K.; Akbari, S.; Harness, J.; Guerra, L.; Frazier, T.; Lane, K.; Simmons, R.; Estabrook, A.; Allweis, T. A randomized prospective study of

lumpectomy margin assessment with use of MarginProbe in patients with nonpalpable breast malignancies. *Annals of Surgical Oncology*, Vol 21 (5), 2014, pp 1589-1595.

[9] Haka, A.; Volynskaya, Z.; Gardecki, J.; Nazemi, J.; Shenk, R.; Wang, N.; Dasari, R.; Fitzmaurice, M.; Feld, M. Diagnosing breast cancer using Raman spectroscopy: prospective analysis. *Journal of Biomedical Optics*, Vol 14 (5), 2009, pp 054023 (1-8).

[10] Keller, M.; Vargis, E.; de Matos Granja, N.; Wilson, R.; Mycek, M.; Kelley, M.; Mahadevan-Jansen, A. Development of a spatially offset Raman spectroscopy probe for breast tumor surgical margin evaluation. *Journal of Biomedical Optics*, Vol 16 (7), 2011, pp 077006 (1-8).

[11] Keller, M.; Majumder, S.; Kelley, M.; Meszoely, I.; Boulos, F.; Olivares, G.; Mahadevan-Jansen, A. Autofluorescence and diffuse reflectance spectroscopy and spectral imaging for breast surgical margin analysis. *Lasers in Surgery and Medicine*, Vol 42 (1), 2010, pp 15-23.

[12] Nguyen, F.; Zysk, A.; Chaney, E.; Kotynek, J.; Oliphant, U.; Bellafiore, F.; Rowland, K.; Johnson, P.; Boppart, S. Intraoperative evaluation of breast tumor margins with optical coherence tomography. *Cancer Research*, Vol 69 (22), 2009, pp 8790–8796.

[13] South, F.; Chaney, E.; Marjanovic, M.; Adie, S.; Boppart, S. Differentiation of ex vivo human breast tissue using polarization-sensitive optical coherence tomography. *Biomedical Optics Express*, Vol 5 (10), 2014, pp 3417-3426.

[14] Patel, R.; Khan A.; Kamionek, M.; Kandil, D.; Quinlan, R.; Yaroslavsky, A. Delineating breast ductal carcinoma using combined dye-enhanced wide-field polarization imaging and optical coherence tomography. *Journal of Biophotonics*, Vol 6 (9), 2013, pp 679-686.

[15] Doyle, T.; Factor, R.; Ellefson, C.; Sorensen, K.; Ambrose, B.; Goodrich, J.; Hart, V.; Jensen, S.; Patel, H.; Neumayer, L. High-frequency ultrasound for intraoperative margin assessments in breast conservation surgery: a feasibility study. *BMC Cancer*, Vol 11, 2011, pp 444 (1-15).

[16] Layfield, D.; Agrawal, A.; Roche, H.; Cutress, R. Intraoperative assessment of sentinel lymph nodes in breast cancer. *British Journal of Surgery*, Vol 98 (1), 2011, pp 4-17.

[17] Chen, D.; Malyarenko, E.; Seviaryn, F.; Yuan, Y.; Sherman, M.; Bandyopadhyay, S.; Gierach, G.; Greenway, C.; Maeva, E.; Strumban, E.; Duric, N.; Maev, R. Characterization of human breast cancer by scanning acoustic microscopy. *SPIE Proceedings Vol. 8675: Medical Imaging 2013: Ultrasonic Imaging, Tomography, and Therapy*, Lake Buena Vista, Florida, February 9-14, 2013.

[18] Miura, K.; Yamamoto, S. A scanning acoustic microscope discriminates cancer cells in fluid. *Scientific Reports*, Vol 5, 2015, pp 15243 (1-10).

[19] Feleppa, E.; Mamou, J.; Porter, C.; Machi, J. Quantitative ultrasound in cancer imaging. *Seminars in Oncology*, Vol 38 (1), 2011, pp 136-150.

[20] Tadayyon, H.; Sadeghi-Naini, A.; Wirtzfeld, L.; Wright, F.; Czarnota, G. Quantitative ultrasound characterization of locally advanced breast cancer by estimation of its scatterer properties. *Medical Physics*, Vol 41 (1), 2014, pp 012903 (1-12).

[21] Mamou, J.; Coron, A.; Oelze, M.; Saegusa Beecroft, E.; Hata, M.; Lee, P.; Junji Machi, J.; Yanagihara, E.; Laugier, P.; Feleppa, E. Three-dimensional high-frequency backscatter and envelope quantification of cancerous human lymph nodes. *Ultrasound in Medicine and Biology*, Vol 37 (3), 2011, pp 345-357.

[22] Doyle, T.; Tew, A.; Warnick, K.; Carruth, B. Simulation of elastic wave scattering in cells and tissues at the microscopic level. *Journal of the Acoustical Society of America*, Vol 125 (3), 2009, pp 1751-1767.